Protein-Induced Changes in Nonplanarity of the Porphyrin in Nickel Cytochrome *c* Probed by Resonance Raman Spectroscopy†

Jian-Guo Ma,‡ Monique Laberge,§ Xing-Zhi Song,‡ Walter Jentzen,‡ Song-Ling Jia,‡ Jun Zhang,‡ Jane M. Vanderkooi,§ and John A. Shelnutt*,‡

Materials Theory and Computation Department, Sandia National Laboratories, Albuquerque, New Mexico 87185-1349, Department of Chemistry, The University of New Mexico, Albuquerque, New Mexico 87131, and Department of Biochemistry and Biophysics, University of Pennsylvania, Philadelphia, Pennsylvania 19104-6089

Received September 24, 1997; Revised Manuscript Received January 26, 1998

ABSTRACT: The influence of the protein on the nonplanarity of the macrocycle for nickel(II)-reconstituted cytochrome *c* (NiCyt-*c*) has been investigated with pH-dependent resonance Raman and UV−visible absorption spectroscopy and molecular mechanics calculations. The spectra reveal that NiCyt-*c* near neutral pH has axially coordinated Ni, but below pH 3 and above pH 12, four-coordinate species predominate. The shape of the structure-sensitive Raman line ν_{10} of NiCyt-*c* is asymmetric and broad and it changes with pH. This broad line can be decomposed well into at least two sublines, a low-frequency line that results from a nonplanar conformer and a high-frequency line that arises from a nearly planar conformer. Upon lowering the pH from 3.0 to 1.0, the amount of the nonplanar conformer decreases relative to that of the planar conformer. The decreased nonplanarity can be accounted for in terms of the disruption of a hydrogen-bonding network in the peptide backbone upon lowering the pH. Molecular mechanics (MM) calculations on iron(III) and nickel(II) microperoxidase 5 (MP-5) as well as some model heme derivatives have been carried out in order to locate the part of the protein that causes the heme distortion observed in the X-ray crystal structures of cytochromes *c*. The energy-optimized structures of MP-5 and the model compounds were analyzed using the normal-coordinate structural decomposition method to specify and quantify the out-of-plane macrocyclic distortions. MM calculations for MP-5 show that two hydrogen bonds formed between the amide groups in the peptide backbone are important in maintaining the ruffled deformation of the macrocycle. All evidence presented supports the hypothesis that the nonplanar distortion of the porphyrin of cytochromes *c* is largely maintained by a relatively small protein segment including the cysteines, the amino acids between the cysteines, and the adjacent histidine ligand. Hydrogen bonding within the backbone of this segment is important in maintaining the conformation of the peptide that induces the porphyrin distortion.

It has been recognized recently that the hemes in many hemoproteins are highly distorted from planarity and that their nonplanar distortions might play a role in their biological function (*1*−*7*). For example, in related photosynthetic proteins, nonplanar distortions have been suggested to influence redox properties of chlorophyll pigments, with consequent effects on electron-transfer rates in photosynthetic reaction centers and antennae complexes (*2*). More recently, by using a new method for characterizing and quantifying these distortions, our group has found that these distortions are often of different types for proteins with different functions, and the types of distortion are conserved for proteins isolated from different species (*8*, *9*). This suggests even more strongly that the biological function of hemoproteins might be modulated by protein control over the conformation of the heme prosthetic group. The importance of nonplanar distortions of the heme is also emphasized by recent studies of model porphyrins showing that hemes are expected to be nearly planar in the absence of the protein moiety; i.e., the nonplanar distortions of the porphyrin macrocycle are induced by the protein environment (*8*, *10*, *11*). It is reasonable to suggest that changes in the protein moiety may influence the nonplanarity of the macrocycle, and protein-induced changes in the nonplanarity may provide a mechanism for protein modulation of biological properties.

One of the approaches used in determining the functional significance of nonplanar heme distortions in proteins is to relate the protein's primary, secondary, and tertiary structure to the establishment of a particular heme conformation. In this regard, many nonplanar model porphyrins, in which the degree of nonplanarity depends on the extent of steric crowding of the peripheral substituents, have been investigated to simulate the role of the protein environment in bringing about nonplanar distortions (*12*−*22*). In this work, we take a more direct approach. Nickel-reconstituted cytochrome *c* (NiCyt-*c*)[1] was chosen to study the effect of pH-dependent changes in protein folding on the nonplanarity of the Ni−protoporphyrin macrocycle. NiCyt-*c* is a good

† Sandia is a multiprogram laboratory operated by Sandia Corporation, a Lockheed Martin Company, for the United States Department of Energy under Contract DE-AC04-94DP85000.

* To whom correspondence should be addressed.
‡ Sandia National Laboratories and The University of New Mexico.
§ University of Pennsylvania.

S0006-2960(97)02375-1 CCC: $15.00
Published on Web 03/25/1998

choice for three reasons: first, NiCyt-*c* has the same tertiary structure as the native protein as judged by electrophoretic mobility and helicity (*23*); second, a great deal of information on model nonplanar nickel porphyrins is available to aid in interpreting the spectral results reliably (*3*−*5*, *13*, *17*, *18*, *21*, *22*); and third and most important, the presence of nickel instead of iron ensures that the proximal histidine will not be coordinated to the metal in the low- and high-pH regions, thus reducing the ambiguity caused by axial ligation in interpreting the spectroscopic results. All of these consequences of nickel replacement help to simplify the spectroscopic features and allow us to focus on the influence of the protein environment on the porphyrin macrocyclic distortion.

Alteration of the solution pH changes the folding state of iron cytochromes *c*. Upon lowering of the pH, the protein becomes progressively less folded in the native tertiary structure, which ultimately results in a less established secondary structure as well (*24*−*27*). These conformational changes of the protein may then have an effect on the out-of-plane conformation of the porphyrin. In this work, pH-dependent resonance Raman (RR) and UV−visible absorption spectra of NiCyt-*c* were obtained to elucidate the capacity of the heme environment to induce nonplanar heme distortions. By utilizing different states of partial protein unfolding, various heme-protein interactions are eliminated. The resulting protein-induced changes in the nonplanarity are evaluated by analyzing the frequency shifts and band shape changes of the structure-sensitive Raman lines, especially ν_{10}. These structure-sensitive Raman lines depend strongly on the degree of nonplanarity of the porphyrin macrocycle, and the band shape of these structure-sensitive lines provide information about structural heterogeneity if present (*10*, *28*, *29*). RR spectroscopy has proven to be one of the best probes of the nonplanar conformation of the porphyrin in solution. In fact, it was the first technique to detect, and the only method currently known that can measure, the conformational equilibrium between coexisting planar and nonplanar forms of metal porphyrins in solution (*10*, *22*, *28*, *29*).

Another feature of the current work is the use of molecular mechanics (MM) calculations to identify and quantify the interactions between the heme and the protein that give rise to the nonplanar distortions. For the cytochromes *c*, a specific pentapeptide segment including the cysteines and the proximal histidine is thought to be involved in causing the out-of-plane distortion (*9*). Thus, the heme and this specific covalently attached protein segment were energy-minimized to predict the structure of the macrocycle. The peptide segment length was varied and various interactions between the heme and protein and within the protein component itself (e.g., hydrogen bonding) were turned on or off in the energy minimization to examine their influence on heme structure.

MATERIALS AND METHODS

Materials. Nickel-reconstituted Cyt-*c* was prepared as follows: Horse heart Cyt-*c* (Sigma Chemical Co.) was depleted of iron and purified as previously described (*30*). Nickel was then incorporated into the metal-free Cyt-*c* according to the procedure of Findlay and Chien (*23*). An equal volume of a solution of 0.2 M nickel acetate, 0.6 M glycyl glycine, and 4 M KSCH at pH 7 was mixed with 0.2 mM iron-free Cyt-*c*. The solution was incubated at 70 °C for 20−25 min, during which time the reaction was monitored by changes in the absorption spectra. The reaction was stopped by dialysis against water at 4 °C. The protein was purified by a Diaflo protein concentrator.

Solutions of the protein at different pH values were used for obtaining spectra. The solutions used in this work are buffered with phosphate (pH > 3.0). Different pH values of the sample solutions were adjusted by KOH or HCl. For pH below 3.0, the buffer used is KCl solutions adjusted with HCl. The NiCyt-*c* solutions are stable in air and do not photodecompose except above pH 12.

Nickel(II) protoporphyrin IX (NiProtoP) was obtained from Porphyrin Products and used without further purification. All solvents were of the highest purity obtainable from commercial sources (Aldrich Chemical Co.).

UV−Visible Absorption Spectroscopy. UV−visible absorption spectra were measured with an HP8452 diode array spectrophotometer (Hewlett-Packard). For conformational transition measurements, Soret absorption spectra of NiCyt-*c* were obtained at protein concentrations of 15 μM with a 0.5-cm path length cell. The protein concentration was determined spectrophotometrically. The extinction coefficient of 150.6 mM^{-1} cm^{-1} at 425 nm was used to calculate the concentration of NiCyt-*c* (*24*). During the titration, the chloride concentration was maintained between 0.46 and 0.50 M. Absorbance values were corrected for dilution resulting from the addition of the concentrated KOH solution. Protein samples at different pH values were prepared before measurement and used as soon as possible. The pH of the NiCyt-*c* samples was measured with a Fisher Accumet Model 50 pH meter. All spectra were taken at room temperature. The peak positions of the absorption bands were obtained by fitting the absorption spectra with Gaussian or Lorentzian lines. The estimated error in the relative band positions is ±1 nm.

Resonance Raman Spectroscopy. RR spectra were obtained using a dual-channel spectrometer described previously (*31*). The solution spectra of porphyrin or NiCyt-*c* and reference compounds were obtained simultaneously in separate compartments of a cylindrical rotating quartz cell. Rotation of the Raman cell at 50 Hz prevented local heating of the sample even with incident laser powers as high as 100 mW. A krypton ion laser (Coherent, INNOVA 20) provided the excitation wavelength (413.1 nm) in the Soret band regions of the absorption spectrum. The scattered light was collected in the 90° scattering geometry. Polarized spectra were measured by passing the scattered light through a Polaroid sheet oriented parallel or perpendicular to the incident-light polarization vector followed by a scrambler in front of the spectrometer entrance slit. The slit width of the spectrometer gave a spectral resolution of 5 cm^{-1} for all spectra.

The solution samples were added to each side of a two-compartment Raman cell. Laser powers were 60 mW at the quartz cell. On each scan of the range from 1300 to 1700 cm^{-1}, counts were accumulated for 1 s at each point of the spectrum for which the spectrometer step size was 0.3 cm^{-1}

[1] Abbreviations: Cyt-*c*, cytochrome *c*; RR, resonance Raman; MP-5, microperoxidase 5; NSD, normal-coordinate structural decomposition; ProtoP, protoporphyrin IX; CTAB, cetyltrimethylammonium bromide.

for each data point. All Raman spectra were taken at room temperature. Sample integrity was monitored by examination of selected single scans of the Raman spectrum obtained during signal averaging and by UV−visible absorption spectra taken before and after exposure to laser light. No degradation of the sample was observed for all measurements.

The frequency calibration of the solution spectra in the region above 900 cm^{-1} was carried out by using the 1373.3-cm^{-1} line of NiTPP in carbon disulfide. The spectra of NiTPP were calibrated with the 992.0-cm^{-1} line of benzene (*32*). Additionally, all spectra were corrected for nonlinearity of the spectrometer to obtain the absolute frequency position of the lines.

The peak positions and full line widths of the Raman lines were obtained by decomposing the Raman spectra into Lorentzian line shapes using a nonlinear least-squares curve-fitting program (PeakFit, Jandel Scientific) in which the peak frequency, peak intensity, line width, and a linear background were allowed to vary. The ν_{10} Raman line of NiCyt-*c* at low pH showed anomalously broad, asymmetric line shapes; thus, two Lorentzian components were used in fitting this line.

Molecular Mechanics Calculations. Molecular mechanics calculations were carried out using POLYGRAF (version 3.21) software (Molecular Simulation, Inc.) and displayed on a Silicon Graphics workstation. The force constants were based on a normal coordinate analysis for NiOEP (*33*−*36*) and the DREIDING II force field (*37*). Equilibrium bond distances, angles, torsions, and inversions were adjusted to reproduce the crystal structure of the triclinic B form of NiOEP (*38*), using a force field optimization routine. The force field for nickel porphyrins has been described in detail elsewhere (*13*) and has been adapted for other metals (*18*). Partial atomic charges used in determining the contribution of the electrostatic energy to the total energy were calculated using the charge equilibration method of Rappé and Goddard (*39*). Electrostatic charges were updated periodically during the energy minimizations. Recently, molecular modeling of porphyrins has reached new levels of accuracy in the calculation of porphyrin structures and conformational energies using a modified version of the force field (*22*). The main modification was the 50% reduction in the out-of-plane force constants. This improved version of the force field is used here, except that a dielectric constant of 79 was used to mimic the solvent environment.

Normal-Coordinate Structural Decomposition. A method for classifying and quantifying the out-of-plane and in-plane distortions of the porphyrin macrocycle has been developed by Jentzen and Shelnutt (*40*). In its simplest form, the NSD method uses a linear combination of the six lowest-frequency out-of-plane normal coordinates of the macrocycle, one of each D_{4h} symmetry type, to simulate the macrocyclic distortion. In most cases, macrocyclic distortions can be described adequately by summing displacements along these six out-of-plane normal coordinates denoted *sad*, *ruf*, *dom*, *wav(x)*, *wav(y)*, and *pro*. Pure displacements along these coordinates correspond to the commonly observed symmetric deformations seen in X-ray crystal structures. The amounts of the saddling (*sad*), ruffling (*ruf*), doming (*dom*), waving [*wav(x)* and *wav(y)*], and propellering (*pro*) deformation types required to simulate the observed out-of-plane distortions of the porphyrin macrocycle are determined for a given structure by the NSD procedure. The NSD method has been successfully used in decomposing and analyzing the structures of hemes of proteins in the Protein Data Bank (*9*) and of synthetic porphyrins (*22*). In this work, the energy-minimized structures of MP-5 and porphyrin model compounds were analyzed using the NSD method to classify and quantify their out-of-plane distortions.

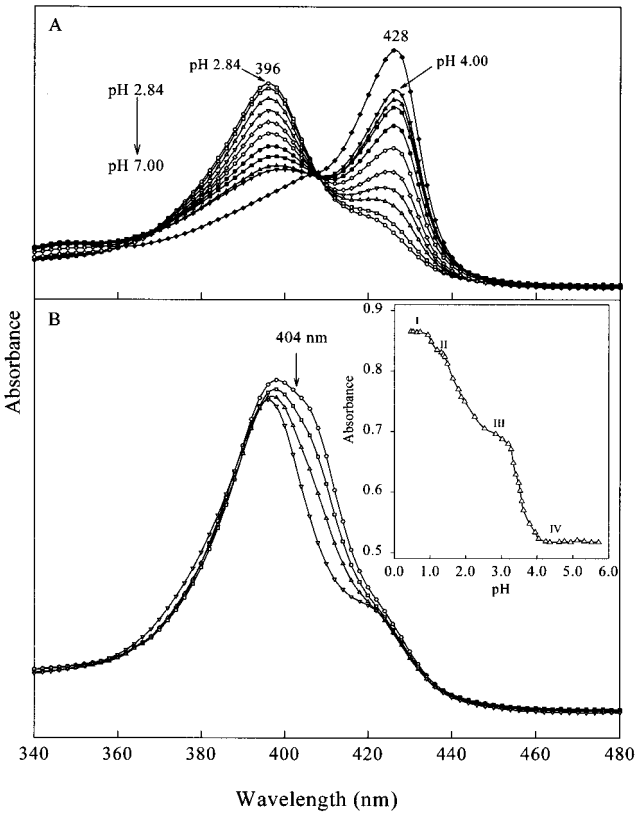

FIGURE 1: Soret band region of the absorption spectrum of NiCyt-*c* at different pH values [in panel B, (○) pH 0.46; (□) pH 1.03; (△) pH 1.64; (▽) pH 2.84]. The inset in panel B indicates the absorbance at 404 nm (△) as a function of pH at constant chloride concentration for NiCyt-*c*. Labels I−IV indicate four different states of NiCyt-*c* in solution. There are three transitions between these four states, i.e., state IV ↔ state III with p$K_a \cong 3.5$, state III ↔ state II with p$K_a \cong 2.0$, and state II ↔ state I with p$K_a \cong 1.1$.

RESULTS

Optical Absorption Spectra. The $\pi-\pi^*$ transitions of the macrocycle give rise to the bands in the UV−visible region of the absorption spectrum, including the B (Soret) band near 400 nm and the Q (α and β) bands in the red region of the visible spectrum. At neutral pH, NiCyt-*c* has the α, β, and Soret band absorption maxima at 579, 546, and 428 nm, respectively. At pH extremes (pH 1.0 and 13.3), the Soret bands of NiCyt-*c* are blue-shifted about 30 nm compared to that of the protein at neutral pH, as observed previously (*23*). The α and β bands exhibit similar blue shifts, and the intensity ratio of the β/α bands inverts for NiCyt-*c* at neutral pH compared to the pH extremes (*23*).

The loss of the axial ligands in acidic solution (*23*), as well as two additional acidic conformational transitions of NiCyt-*c*, have been identified in the present work. Figure 1 shows the results of titration of NiCyt-*c* in the Soret band region for the pH range from pH 0.5 to 7.0. The two Soret

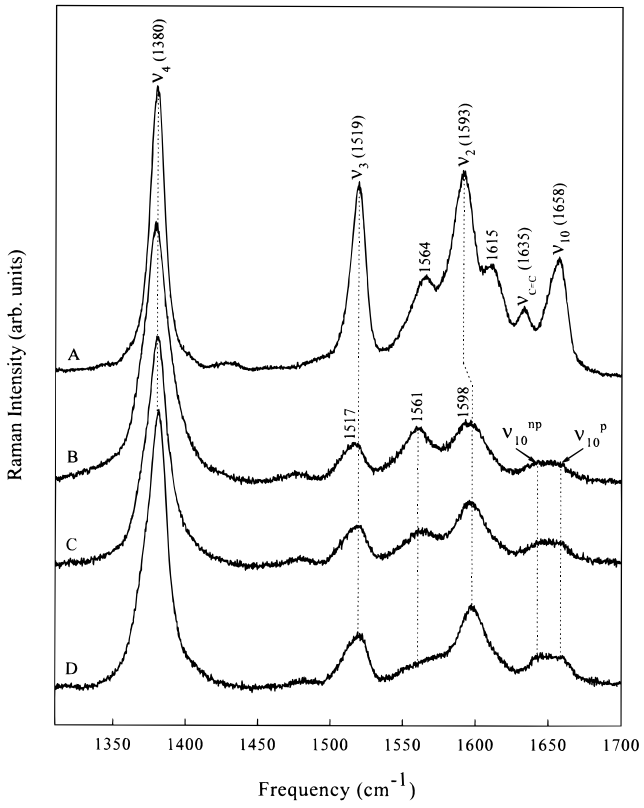

FIGURE 2: Resonance Raman spectra of NiProtoP in CTAB micelles (A) and NiCyt-*c* at pH 1.0 (B), 2.0 (C), and 3.0 (D) with 413.1-nm excitation.

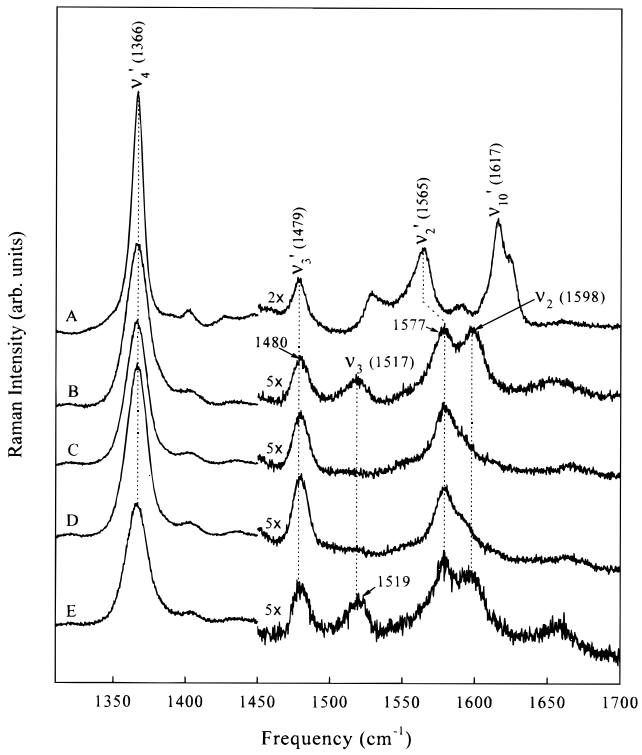

FIGURE 3: Resonance Raman spectra of NiProtoP in pyrrolidine (A) and NiCyt-*c* at pH 3.9 (B), 7.0 (C), 9.0 (D), and 11.0 (E) with 413.1-nm excitation. (ν_4', ν_3', ν_2', and ν_{10}' are structure-sensitive Raman lines of the axial-ligated species; ν_3 and ν_2 are structure-sensitive Raman lines of the four-coordinate species.)

bands found in the pH range from pH 2.8 to 4.0 are at 396 nm, corresponding to four-coordinate NiCyt-*c*, and at 428 nm, corresponding to the axially ligated form. The transition occurring in the pH region from 4.0 to 2.8 with increasing intensity of the Soret band at 396 nm previously observed by Findlay and Chien (*23*) corresponds to the loss of axial ligands.

Examination of the Soret bands of NiCyt-*c* at the four different pH values shown in Figure 1B shows that additional changes occur in this very low pH region. In particular, the Soret band at pH 0.5 is broader than that for the other three pH values. In addition, the absorbance at 404 nm decreases significantly as the pH is raised from 0.5 to 2.8. It is thought that at least two forms exist in this pH range on the basis of these spectra. These two forms are both four-coordinate and probably differ in the conformation of the porphyrin macrocycle. To inspect this conformational transition more clearly, we plotted the absorbance at 404 nm in the pH range from 0.5 to 5.8 as shown in the inset in Figure 1B. It is clear from the inset that the acidic pH transition of NiCyt-*c* in the presence of chloride at constant concentration is a three-step, four-species process, i.e., state IV ↔ state III ↔ state II ↔ state I, with pK_as of about 3.5, 2.0, and 1.1, respectively. State IV corresponds to the axial-ligated species of NiCyt-*c*, while states III, II, and I are four-coordinate and differ in the conformation of the porphyrin.

Resonance Raman Spectra. Figure 2 shows the high-frequency region of the RR spectra of NiCyt-*c* at pH 1.0, 2.0, and 3.0 and NiProtoP in CTAB micelles. The RR spectra of NiCyt-*c* at pH 3.9, 7.0, 9.0, and 11.0 and NiProtoP in pyrrolidine are shown in Figure 3. The frequencies of major Raman lines of these spectra are indicated. Most of the structure-sensitive Raman lines including ν_4, ν_3, ν_2, and ν_{10} are within this spectral region. These lines are labeled according to the normal coordinate analysis of NiOEP (*33*−*36*) and correspond to in-plane skeletal vibrations of the macrocycle having A_{1g} and B_{2g} symmetries in the D_{4h} point-group representation.

Large downshifts in the Raman line frequencies are observed in the near neutral pH forms of NiCyt-*c* (Figure 3B−D) relative to the protein at lower pH (Figure 2B−D). For NiCyt-*c* at near neutral pH, the frequencies of the Raman marker lines, ν_4, ν_3, and ν_2 are downshifted by about 14, 37, and 21 cm^{-1} compared to NiCyt-*c* at pH extremes (Figure 2B). At pH 1.0, 2.0, and 3.0 (Figure 2 panels B, C, and D), the frequencies of ν_4 and ν_3 for NiCyt-*c* are close to those observed for NiProtoP in CTAB micelles (Figure 2A), which is a four-coordinate model (*41*). The frequencies of ν_4 and ν_3 for NiCyt-*c* at near neutral pH are close to those observed for NiProtoP in pyrrolidine (Figure 3A), which is a six-coordinate model (*41*). The spectra of NiCyt-*c* at pH 3.9 and 11.0 both show two ν_3 lines (1480 and 1517 cm^{-1}) and two ν_2 lines (1577 and 1598 cm^{-1}) that correspond to the axially ligated and four-coordinate forms of NiCyt-*c*, respectively.

The frequencies of ν_2 of NiCyt-*c* at pH 1.0, 2.0, and 3.0 exhibit small upshifts ($\sim$ 5 cm^{-1}) compared to the model compound (Figure 2). This can be accounted for by the reduction of two vinyls of the heme in Cyt-*c*. Reduction of the vinyls leads to decoupling of the ν_2 mode and the vinyl stretching mode and results in a frequency increase of ν_2 (*42*, *43*). These upshifts of the ν_2 mode are also observed in the spectra of NiCyt-*c* at pH 3.9, 7.0, 9.0, and 11.0 (Figure 3B−E) relative to the spectrum of six-coordinate models

Table 1: Frequencies and Other Spectral Parameters for the ν_{10} Line of the Four-Coordinate Sites of Nickel-Reconstituted Cytochrome *c* and Ni Protoporphyrin IX[a]

	frequency (cm^{-1})			line width			relative areas ($\nu_{10}^{np}/\nu_{10}^{p}$)		
mode	NiPP[b]	NiCyt-*c* (pH 1.0)	NiCyt-*c* (pH 3.0)	NiPP	NiCyt-*c* (pH 1.0)	NiCyt-*c* (pH 3.0)	NiPP	NiCyt-*c* (pH 1.0)	NiCyt-*c* (pH 3.0)
ν_{10}^{np}	1652.8 ± 0.2	1646.7 ± 0.6	1645.9 ± 0.4	12.7 ± 0.3	20.9 ± 0.7	25.4 ± 0.6	0.6	2.1	3.8
ν_{10}^{p}	1659.9 ± 0.1	1659.8 ± 0.4	1659.9 ± 0.3	11[c]	11[c]	11[c]			

[a] The errors indicated represent confidence levels for the least-squares fits, not true errors. [b] The spectrum was taken in CTAB micelles. [c] The line width was fixed in the curve fitting. ν_{10}^{np} is the ν_{10} line of the nonplanar conformer; ν_{10}^{p} is the ν_{10} line of the nearly planar conformer.

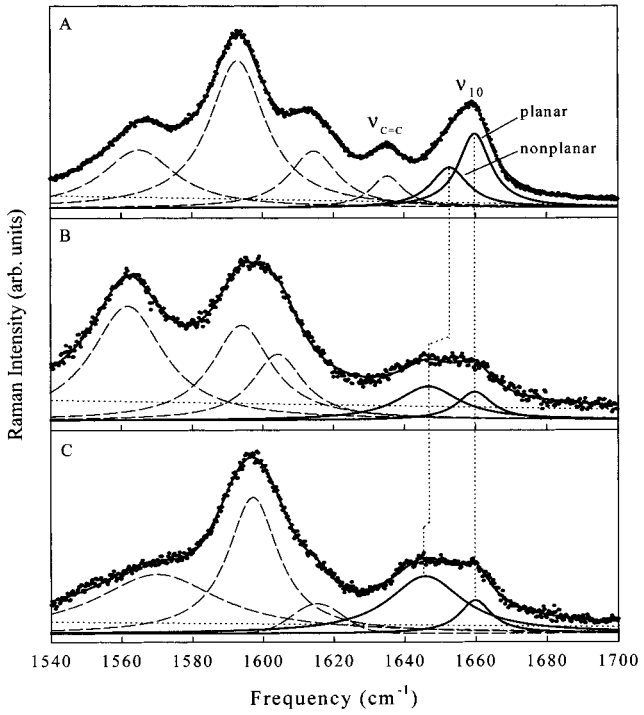

FIGURE 4: Lorentzian decomposition of the ν_{10} resonance Raman lines in the spectra of NiProtoP in CTAB micelles (A) and NiCyt-*c* at pH 1.0 (B) and 3.0 (C). The line width of the high-frequency component of ν_{10} was fixed at 11 cm^{-1}. All other line parameters were allowed to vary in the curve fit. Spectra B and C were obtained simultaneously on the Raman difference spectrometer with 413.1-nm excitation.

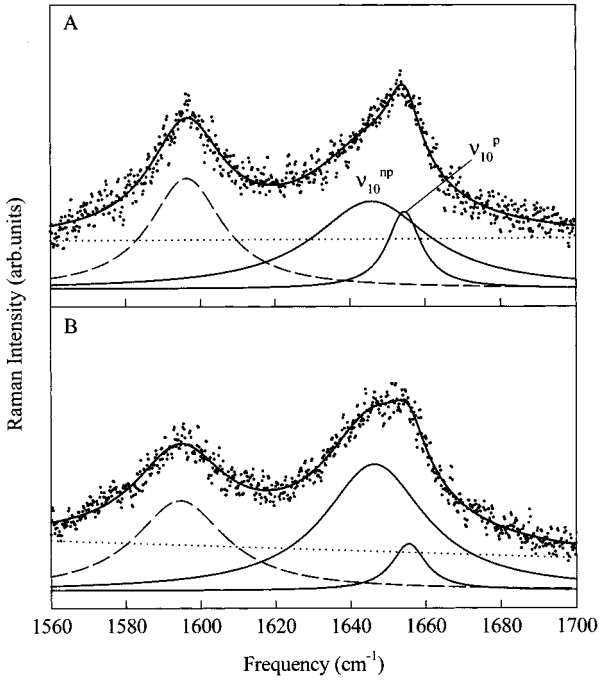

FIGURE 5: Lorentzian decomposition of the ν_{10} resonance Raman line in the perpendicularly polarized RR spectra of NiCyt-*c* taken at pH 1.0 (A) and 3.0 (B). The line width of the high-frequency component of ν_{10} was fixed at 11 cm^{-1}. All other line parameters were allowed to vary in the curve fit.

such as NiProtoP in pyrrolidine (Figure 3A). These upshifts are also observed for nickel mesoporphyrin models (*11*).

In comparison with the four-coordinate model compound, the line shapes of ν_3, ν_2, and ν_{10} for NiCyt-*c* at pH 1.0, 2.0, and 3.0 are broader and more asymmetric. This broadening indicates structural heterogeneity of NiCyt-*c* in solution. The spectral trend in this structural heterogeneity with pH is very interesting. Unfortunately, only the ν_{10} region of the spectrum is suitable for spectral analysis, since the ν_2 region suffers from spectral crowding and ν_3 is relatively less sensitive to porphyrin nonplanarity than ν_{10}. Upon raising of the pH from 1.0 to 3.0, the line shape of ν_{10} becomes more asymmetric; thus, a more detailed examination of the composition of the ν_{10} line was then undertaken. Figure 4 shows the Lorentzian decomposition of the 1540−1700 cm^{-1} region of the spectra of NiCyt-*c* at pH 1.0 and 3.0 obtained simultaneously at 413.1-nm excitation using the dual-channel Raman spectrometer. The Lorentzian decomposition of the RR spectrum of NiProtoP in CTAB micelles is also shown for comparison. In curve fitting, the line width of ν_{10} for the high-frequency component was fixed at 11 cm^{-1}, while all other line parameters were allowed to vary. This 11-cm^{-1} width is reasonable for a planar conformer in solution (*5*, *29*) and is comparable to the width observed for Raman spectra of crystals of metal octaethylporphyrins (*10*). Best-fit parameters for ν_{10} are given in Table 1. The trend in the intensity ratios is an increase of the ratio with pH, and this trend holds for other Raman spectra (not shown), e.g., spectra taken at intermediate pH values between 1 and 3. Particularly convincing is the spectral decomposition of the perpendicularly polarized spectra in the 1560−1700 cm^{-1} region shown in Figure 5. The intensity of ν_2 is greatly reduced relative to ν_{10} in these spectra, thus improving the line-shape analysis. In these spectra, the trend toward decreasing nonplanarity at low pH (pH 1) is unambiguous, even without the aid of spectral decompositions. At pH 1, the nonplanar-to-planar ratio of the components of ν_{10} obtained from the spectral decompositions is decreased by about a factor of 2 compared to the ratio at pH 3.

The intensity of the Raman line at 1561 cm^{-1} (Figure 2B) decreases as the pH is raised from 1.0 to 3.0. The assignment of this line is not definite at present, but it may be related to the conformational change of the thioether and other sub-

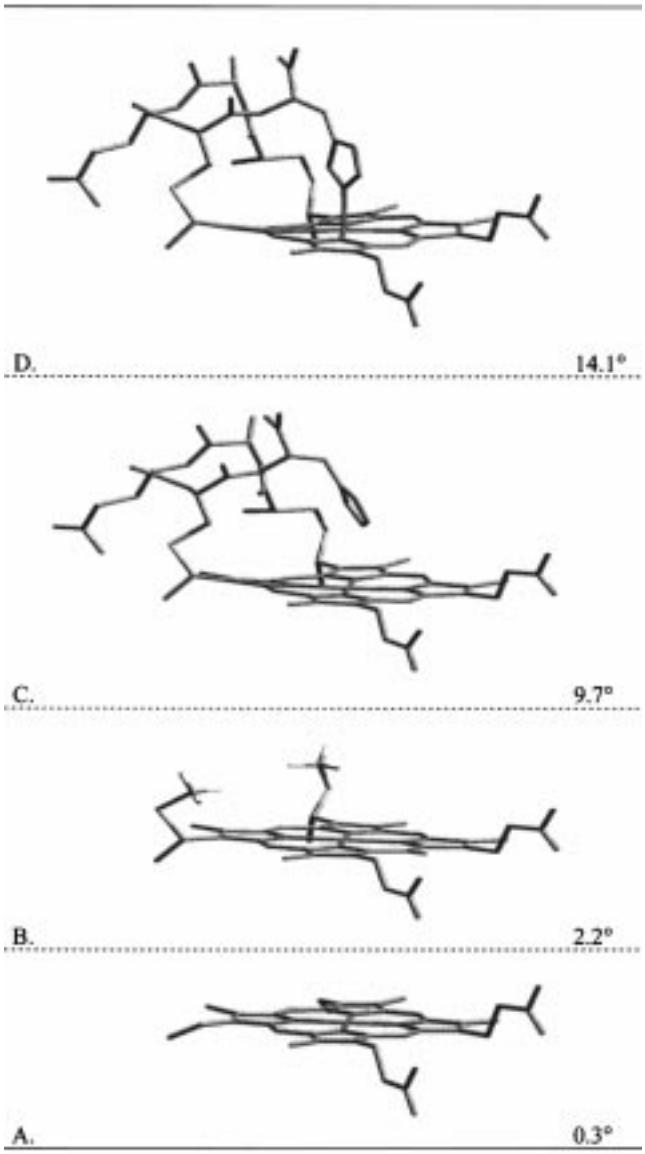

FIGURE 6: Representation of energy-minimized structures of Fe(III) ProtoP (A), Fe(III) ProtoP-di(methylthioether) (B), Fe(III) MP-5 with unbound histidine (C), and Fe(III) MP-5 with bound histidine (D) showing effects of various 2- and 4- substituents and interactions on the $C_\alpha-N-N-C_\alpha$ ruffling dihedral angle of opposite pyrrole planes. The numbers shown are the ruffling dihedral angles.

stituents of the porphyrin. However, it is probably not ν_{11} since the line is polarized.

The low-frequency region between 200 and 500 cm^{-1} contains numerous pH-dependent changes; some, like the changes in ν_8, are consistent with the structural change indicated by the high-frequency structural marker lines. The low-frequency region will be the focus of a forthcoming paper.

Molecular Mechanics Calculations and Normal-Coordinate Structural Decompositions. MM calculations greatly aid in locating the protein forces that maintain the nonplanar macrocyclic distortion. To evaluate the effect of the various influences on the porphyrin macrocycle of NiCyt-*c*, we carried out MM calculations on hypothetical Fe(III) microperoxidase (MP) and model compounds [ProtoP and ProtoP-di(methylthioether)] that vary in the size and properties of the segment covalently attached to the macrocycle. The energy-minimized structures of these compounds are illustrated in Figure 6. The influences of the histidine ligand on the nonplanarity of the porphyrin macrocycle are evaluated by deleting the Fe−histidine bond in some energy minimizations.

Table 2: Energies and Structure Parameters for Energy-Optimized Fe(III) and Ni(II) Microperoxidase 5 (MP-5) and Model Compounds

porphyrin[a]	histidine	H bonds[b]	energy (kcal/mol)	core size (Å)	twist angle (deg)	N−M−N angle (deg)
Fe(III) MP-5[c]	bound	on	162.8	1.9998	14.1	176.8
		off	172.1	2.0015	12.0	176.6
	unbound	on	161.3	2.0028	9.7	177.2
		off	171.1	2.0040	8.6	177.2
Fe(III)ProtoP-methylsulfide[d]			126.3	2.0073	2.2	179.7
Fe(III)ProtoP			127.3	2.0072	0.3	179.8
Ni(II) MP-5[c]	unbound	on	165.4	1.9397	24.0	179.2
		off	175.1	1.9424	21.9	178.5

[a] The initial structures used in the calculations were obtained from the X-ray crystal structure of horse heart ferricytochrome *c*. [b] The hydrogen bonds among amino acid residues were either kept (turned on) or omitted (turned off) in the minimization. [c] Amino acid sequence is -Cys14-Ala15-Gln16-Cys17-His18-. [d] The vinyl groups of Fe(III)-ProtoP were modified by two methylthioether groups.

Nonbonding interactions between the protein and macrocycle, namely, electrostatic, hydrogen bonding, and van der Waals interactions, are also expected to be important in determining the types, the magnitudes, and the relative energies of the distortions. To directly address the distortion effect of hydrogen bonding in the peptide, we also carried out calculations in which the hydrogen bonds were turned on or off for Fe(III) and Ni(II) MP-5. The calculated structural parameters for Fe(III) and Ni(II) MP-5 and the model Fe(III) porphyrins are summarized in Table 2.

The initial structures of MP-5 used in MM calculations were built according to the X-ray crystal structure of horse heart ferricytochrome *c* by deleting the peptide except for the CAQCH pentapeptide unit attached to the heme. The heme−pentapeptide and model compounds were energy-optimized and the resulting nonplanar macrocycle conformation is measured by several parameters. The N−M−N bond angle across the porphyrin (opposite pyrrole nitrogens) is related to the amount of pyrrole tilting in the saddling (*sad*) and doming (*dom*) distortions of the metalloporphyrin. In the *sad* form, the *meso*-carbons (C_m) remain in the mean porphyrin plane and the pyrrole rings are alternately displaced above and below the mean plane. The ruffling (*ruf*) of the macrocycle, induced by opposite twisting of the pyrroles about the M−N bonds, is measured by the $C_\alpha-N-N-C_\alpha$ dihedral angles, called the twist angle in Table 2. These two angles quantify these general types of distortion observed in metalloporphyrins (*19*, *44*). The core size as defined here is the projection of the M−N bond into the average plane of the macrocycle.

The effects of the attached protein segment on the heme distortion are illustrated in Figure 6. First, panel A of Figure 6 shows the energy-optimized structure of Fe(III)ProtoP, which is almost planar (average pyrrole ruffling dihedral angle is less than 1°). Panel B shows the effect of thioether modifications of the vinyl substituents of Fe(III)ProtoP. The macrocycle is slightly more distorted than that of Fe(III)-ProtoP because of the increased bulkiness of the substituents (average pyrrole ruffling dihedral angle is 2.2°). Panel C in

Table 3: Out-of-Plane Displacements of the Minimal Basis for the Energy-Minimized Structures of Fe(III) MP-5, Ni(II) MP-5, Model Compounds, and the Horse Cytochrome *c* Crystal Structure

conformer[a]	histidine	H bonds[a]	out-of-plane displacements (Å)						
			D_{oop}[b]	*ruf*	*sad*	*dom*	*wav(x)*	*wav(y)*	*pro*
cytochrome *c*			1.049	1.004	−0.224	−0.020	0.122	0.161	−0.022
Fe(III) MP-5	bound	on	0.763	0.682	0.301	0.069	0.071	0.108	0.072
		off	0.767	0.582	0.487	0.016	−0.007	0.095	0.059
	unbound	on	0.540	0.471	0.027	0.188	0.120	0.122	0.065
		off	0.477	0.418	0.146	0.135	0.043	0.083	0.068
Fe(III)ProtoP-methylsulfide			0.136	−0.104	0.063	0.009	−0.043	0.011	0.041
Fe(III)ProtoP			0.068	0.002	0.036	−0.006	−0.025	0.052	0.000
Ni(II) MP-5	unbound	on	1.165	1.144	0.152	0.113	0.053	0.064	0.077
		off	1.108	1.049	0.336	0.075	−0.015	0.056	0.067

[a] Legends are the same as in Table 2. [b] Simulated total out-of-plane displacement.

Figure 6 shows the effect of the CAQCH pentapeptide unit on the heme conformation where the His-Fe bond is absent (ruffling angle is 9.7°). And finally, panel D shows the effect of the pentapeptide unit when the His−Fe bond is present. In the latter case, the ruffling angle is 14.1°, very close to the average ruffling angle for all of the available X-ray crystal structures of the mitochondrial cytochromes *c* (*8*).

Analysis of the pyrrole twist angles (see Table 2) for the energy-minimized structures of Fe(III) and Ni(II) MP-5 and the model compounds indicates that, in the absence of hydrogen bonding, the macrocycle minimizes to a less ruffled conformation than that observed in the presence of hydrogen bonding. That is, the twist angle of the macrocycle in the absence of the hydrogen bonds is smaller than that of the macrocycle in the presence of the hydrogen bonds. The hydrogen-bond effect likely would be even larger were the solvent (water) molecules included explicitly in the MM calculations.

Ruffling is the major distortion of the heme, but other structural parameters (core size and N−M−N angle) in Table 2 also illustrate the effects of the attached protein segments on macrocyclic distortion. For Fe(III) MP-5 and model compounds, the core size of each conformer increases as the ruffling angle decreases, as expected. In addition, the Ni(II) derivatives have a smaller core size than Fe(III) MP-5 as expected for the small Ni ion. Also, the N−M−N saddling angle changes with increased size of the peptide segment; the saddling angle is 179.8° for Fe(III) ProtoP, decreasing to 176.8° for Fe(III) MP-5 (His bound). The decrease in the N−M−N angle is primarily the result of increased saddling of the macrocycle. At this point, we can conclude that the protein segment makes the macrocycle more distorted, increasing the ruffling and saddling.

Actually, the conformation of the porphyrin macrocycle is a complex mixture of several types of distortions (e.g., ruffling, saddling, doming, and waving). The NSD method developed recently (*40*) provides us a means to quantify the contributions of these out-of-plane deformations to the total distortion of the macrocycle in detail. The contribution of each basic deformation [*ruf*, *sad*, *dom*, *wav(x)*, *wav(y)*, and *pro*] to the total distortion of the macrocycle is obtained by decomposing the energy-minimized structures using the NSD method. Table 3 lists the displacements along out-of-plane normal coordinates that best simulate (using the minimal basis) (*40*) the energy-minimized structures. The energy-minimized structure of Fe(III)ProtoP is almost planar as indicated by the total root square out-of-plane displacement (0.068 Å). After thioether modifications of the vinyl substituents of Fe(III)ProtoP, the macrocycle becomes more distorted (D_{oop} = 0.136 Å). Upon examination of the out-of-plane displacement for the types of deformation, one finds that ruffling is already the major contributor (−0.104 Å) to the distortion. Furthermore, with the CAQCH pentapeptide attached, the total out-of-plane displacement increases significantly (D_{oop} > 0.477 Å). Adding Fe−His bond and the hydrogen bonding in the peptide brings the total distortion to 0.8 Å.

For both Fe(III) MP-5 (His bound and unbound) and Ni(II) MP-5 (His unbound), the main type of deformation is *ruf*, although *sad* is an important secondary contributor. Interestingly, if one deletes the His−Fe bond for Fe(III) MP-5, the saddling displacement decreases drastically (from 0.301 to 0.027 Å) and the ruffling displacement also decreases (from 0.682 to 0.471 Å). Surprisingly, doming actually decreases when the histidine is bound. Both *wav(x)* and *wav(y)* are more evident when hydrogen bonding in the peptide is turned on. The propeller displacements are not significant for all the minimized structures. The NSD results (*9*) of the crystal structure of horse heart cytochrome *c* (*45*) are shown in Table 3 for comparison.

DISCUSSION

The Coordination State of NiCyt-c Is pH-Dependent. It is well-known that the Soret-band wavelength is sensitive to axial ligands of the metal that interact indirectly with the π-electron system of the porphyrin (*43*, *46*, *47*). At neutral pH, NiCyt-*c* has its Soret band red-shifted compared to that of the protein at pH extremes (pH 1.0 and 13.3). The α and β bands of the absorption spectra for NiCyt-*c* exhibit similar red shifts. By comparison of the absorption spectra of NiCyt-*c* with those of model nickel porphyrins and other metal-reconstituted heme proteins (*23*, *41*), the major changes in the absorption spectrum can be ascribed to the loss of the histidine ligand at low pH (p$K_a \sim 3.5$). More subtle changes in the spectrum are also evident. For example, a shoulder on the low-energy side of the Soret band near 420 nm for NiCyt-*c* at pH 13.3 may indicate a residual concentration of an axially ligated species in the denatured proteins. At present we cannot say with certainty whether the methionine ligand is bound or not at neutral pH. It is certainly not bound strongly, as NiCyt-*c* binds NO as an axial ligand, most likely displacing the methionine if bound (*23*). In fact, NO does

not displace pyridine in model nickel porphyrins in neat pyridine. In addition, the blue shift of the Soret-band maximum relative to some other six-coordinate models suggests that the methionine may not be bound and that Ni could be five-coordinate.

RR studies of NiCyt-*c* at different pH values further elucidate the pH-dependent change in ligation state. From Figures 2 and 3, the frequencies of the Raman marker lines, ν_4, ν_3, and ν_2, for the neutral pH form of NiCyt-*c* are downshifted by 14, 37, and 21 cm^{-1}, respectively, compared to the protein at pH extremes. It has already been shown that the pattern of shifts occurring upon addition of ligands is one of large shifts to low frequency for the structure-sensitive marker-lines (-40 cm^{-1}, ν_{10}) and a somewhat smaller shift for the oxidation-state marker line ν_4, also to low frequency (-14 cm^{-1}) (*41*) (Figure 2A and 3A). A comparison of four-coordinate frequencies with those for NiCyt-*c* at pH 7 shows that the shifts are near those expected if σ-donating axial ligands are added. Furthermore, the presence of components of ν_3 and ν_2 from both axially ligated and unligated species at pH 3.9 and 11.0 show that both species of NiCyt-*c* coexist in solution at these pH values. At neutral pH, the axial-ligated species of the protein overwhelmingly dominates.

NiCyt-c and Native Ferricytochrome c Exhibit Similar Acidic Conformational Transitions. Disruption of hydrogen bonding in the peptide backbone at low pH may account for the decreased nonplanar distortion of the macrocycle. Acid-induced folding and unfolding of cytochromes *c* has been studied by several researchers (*24*−*27*, *48*, *49*). For mitochondrial cytochromes *c*, a single heme is covalently attached to the polypeptide by two thioether bridges. In the crystalline state, the polypeptide chain is folded about the heme, forming a nearly spherical molecule with a hydrophobic interior and a hydrophilic exterior (*50*). Hydrogen bonding in the peptide backbone is believed to be important in maintaining the secondary and tertiary structure of the protein. In globular proteins, most hydrogen bonds are between backbone atoms (average of 68%) and most proteins have extensive hydrogen-bonded secondary structure (average of 82%) (*51*). The native conformation of cytochromes *c* in solution as deduced by a variety of physical and chemical measurements is generally the same as that described for the crystalline state (*24*). Addition of acid to the native protein causes a conformational transition from a fully folded environment to a partially unfolded protein (*27*, *48*, *49*). The protein is considered to be less folded than that of the native species in which structural elements, typically secondary structural units, have been pulled apart somewhat, leading to solvent penetration and enhanced side-chain mobility (*25*). In some cases, part of the molecule (e.g., the C-terminal region) may be fully unfolded (random coil).

Spectroscopic studies of ferricytochrome *c* by others (*27*) have demonstrated the presence of at least four conformational states of the native iron protein in the pH region 0.5−7.0. The conversions between the protein conformational states $III_s \leftrightarrow III_{s,a} \leftrightarrow II_s \leftrightarrow I_s$ occur with pK_as of 3.5, 2.2 and 1.1. The state $III_{s,a}$ is folded in about the same way as native III_s, but the heme crevice is loosened. Also, the spin state and coordination configuration of $III_{s,a}$ is similar to that of III_s. The two protein forms below pH 3.0, I_s and II_s, are also folded forms, but with smaller degrees of protein secondary structure and altered axial coordination. State II_s has high-spin six-coordinate heme with the histidine and a water molecule as ligands. State I_s is five-coordinate with histidine as the only ligand.

Similar protein conformational states appear in NiCyt-*c*. First, the pK_a of the histidine or histidine/methionine ligand loss occurs at about pH 3.5, the pK_a of the loosening of the heme crevice in ferricytochrome *c* (see inset in Figure 1B). Second, it was thought that states II_s and I_s might also occur in the nickel protein, disrupting the secondary structure and weakening the hydrogen bonding within the peptide as occurs for the native protein. In particular, we reasoned that disruption of the hydrogen bonds would lengthen the CAQCH segment and possibly decrease the degree of nonplanarity of the porphyrin macrocycle, in accordance with the molecular mechanics calculations. Indeed, changes in the structure of the four-coordinate nickel porphyrin in NiCyt-*c* are evident in the Soret-band spectral changes in the low pH region from pH 0.5 to 2.8 (Figure 1B). These spectral changes clearly indicate that similar protein conformational states exist regardless of the metal. In addition, the absorption spectrum changes in this pH range can be ascribed to increased occupation of a near planar porphyrin conformer as the pH is lowered, consistent with the RR spectra (vide infra). However, it should be noted that more planar forms are usually associated with a blue shift in the Soret band, not a red shift as seen in the very low pH spectra of Figure 1B.

The Amount of the Nonplanar NiCyt-c Conformer Decreases Relative to That of the Planar Conformer As the pH Is Lowered. The spectral region shown in Figure 4 contains the Raman line ν_{10} that is most sensitive to nonplanar distortion of the porphyrin. The region of the spectrum near ν_{10} is not complicated by spectral crowding, as is the rest of the region. Anticipating the presence of multiple forms as the cause of the broadness of ν_{10}, we have resolved ν_{10} into two sublines as shown (solid lines). The high-frequency subline is associated with a nearly planar form based on its frequency (1660 cm^{-1}); the low-frequency sublines are associated with nonplanar forms. Although the resonance excitation difference, resulting from the different absorption spectra of the conformers, influences the relative intensities and thus estimates of concentration, it is clear that both planar and nonplanar forms are very much in evidence for the NiProtoP model compound. Similar ratios of nonplanar-to-planar intensities are observed for other nickel−porphyrin models, including nickel octaethylporphyrin (NiOEP) (*29*) and nickel tetraphenylporphyrin (NiTPP) (*52*).

Most interesting is that the relative intensity of the subline corresponding to the nonplanar form is much greater for NiCyt-*c* at both pH values than for the model compounds (Figure 4). The ratio of intensities (nonplanar/planar) is 0.6 for NiProtoP, 2.1 for NiCyt-*c* at pH 1.0, and 3.8 at pH 3.0 (Table 1). Thus it appears that the equilibrium shifts toward the nearly planar conformer as the secondary structure, i.e., the hydrogen bonding in the peptide backbone, becomes less established around pH 1.0. In addition, on the basis of the lower frequency of the sublines for NiCyt-*c* (1647 cm^{-1} at pH 1.0, 1646 cm^{-1} at pH 3.0) compared to NiProtoP (1653 cm^{-1}), the nonplanar conformers of NiCyt-*c* are considerably more nonplanar than the nonplanar conformers of the model compound. It is well-known (*53*) that differences in the

frequency of ν_{10} are not due to differences in the peripheral substituents. This is apparent also from the near identity of the frequencies of the nearly planar forms (Table 1). More importantly, the degree of distortion of the macrocycle is slightly smaller at the lower pH, as expected if the hydrogen-bonding network in the protein secondary structure is weakened.

It is reasonable to suggest that alteration of the forces that maintain the protein folding will influence the nonplanarity of the porphyrin macrocycle. On increasing the acidity of the solution, residues in the protein become more positively charged. The resulting intramolecular repulsion between the positively charged groups leads to unfolding. Initially, mainly the tertiary structure is affected, but at very low pH a relatively extended conformation with a smaller degree of protein secondary structure results. This disfavors the optimization of the number and geometry of >N−H···O═C< hydrogen bonds in the peptide backbone. Also, the extended conformation allows the solvent molecules to penetrate into the interior of the protein and form hydrogen bonds with the amide groups on the peptide backbone. The penetrating solvent molecules compete with the amide groups in forming the hydrogen bonds that maintain the protein secondary structure. If this occurs in the covalently linked pentapeptide segment, disruption of these hydrogen bonds can reduce the macrocyclic distortion. A similar disruption of the hydrogen-bonding network in the heme pocket is noted in hydrogen−deuterium exchange experiments with cytochrome *c*. The exchange experiments demonstrate that the hydrogen-bonding network sensitively controls the conformation of the porphyrin (*6*).

The CAQCH Peptide Segment Causes Much of the Macrocyclic Distortion for Cytochromes c. The nonplanar distortion of the macrocycle for cytochromes *c* is maintained only in the protein environment; i.e., without the protein environment, the macrocycle will be nearly planar (*8*, *10*). Moreover, a Raman study of Fe(III) MP-8 by Desbois and co-workers (*54*) has shown that the nonplanar conformers observed in the X-ray structures of cytochromes *c* are probably also present in MP-8 in aqueous micellar solution. They conclude that the nonplanar conformation is essentially due to the three-point attachments between the heme and protein, i.e., the two thioether bridges and the Fe−His bond. Indeed, they showed that replacement of the proximal His with an exogenous His ligand results in a less distorted heme, based on the shifts in the frequencies of two structure-sensitive Raman lines, ν_8 and ν_{10}. The use of these lines as markers of the nonplanarity of the porphyrin is based on the known behavior of these lines upon ruffling of nickel porphyrins (*5*, *21*, *28*, *55*).

The molecular mechanics calculations show that the three-point connection of the pentapeptide is sufficient, in fact, to explain most of the normal-coordinate deformations making up the observed distortion of the heme of the cytochromes *c* (*9*). As shown by our calculations on Fe(III) MP-5, the ruffling angle for the pentapeptide is already very close to the average ruffling angle for all available crystal structures of cytochromes *c*. Specifically, for the horse cytochrome *c* crystal structure, the observed ruffling and total distortions are only a little larger than calculated (Table 3). Nevertheless, both the ruffling and waving [$wav(x)$ and $wav(y)$] contributions are qualitatively predicted by the calculated structure of Fe(III) MP-5 (His bound), as can be seen from Table 3. However, the rest of the protein apparently has some effect on the distortion of the macrocycle. For example, the negative saddling deformation is not reproduced by the calculated Fe(III) MP-5 structure. The saddling deformation probably arises from additional heme interactions with the protein (e.g., hydrogen bonding to the propionates) or else from a difference in the conformation of the pentapeptide segment due to its interaction with the rest of the protein. This issue will be addressed in detail in a future report on Ni MP-11 studies (*11*).

The importance of the pentapeptide segment including the cysteines and the proximal histidine in maintaining the heme distortion in cytochromes *c* and c_3 was suggested by Jentzen, Ma, and Shelnutt (*9*, *40*, *56*). Specifically, they noted that the main type of distortion for mitochondrial cytochromes *c* is ruffling. In the cytochromes *c*′, saddling and ruffling are more nearly equal, with saddling dominant for five of the six currently known crystal structures (*9*). Accordingly, examination of the crystal structures of the cytochromes *c*′ showed that the conformation of the pentapeptide segment differs from that in the mitochondrial cytochromes *c*, having only one hydrogen bond in the backbone. Thus, they suggested that the difference in hydrogen bonding could account for the predominance of saddling in the cytochromes *c*′ as opposed to ruffling for the mitochondrial cytochromes *c*. Upon examination of the energy-minimized structure of Fe(III) MP-5, one finds that there are two hydrogen bonds formed between the >C═O and H−N< groups in the peptide backbone. Indeed, when the hydrogen bonding is turned off in the calculation, the optimized structure of five-coordinate Fe(III) MP-5 adopts a more saddled and less ruffled conformation than that of the structure obtained with the hydrogen bonding on. This is also true for four-coordinate Fe(III) and Ni(II) MP-5 (Table 3).

All of our results support the hypothesis that the macrocyclic distortion in cytochromes *c* is mainly caused by the peptide segment, including the cysteines and the proximal histidine. The RR studies on NiCyt-*c* provide experimental evidence that the macrocyclic distortion decreases as the hydrogen-bonding network becomes less established in the peptide backbone. However, even if the protein does show a less distorted porphyrin at very low pH, consistent with our hypothesis, we cannot conclusively show that a particular peptide segment actually causes the heme distortion on the basis of these NiCyt-*c* results alone. The problem is that we cannot say which part of the protein is important, although MM calculations on MP-5 provide some evidence that the CAQCH segment alone can cause the macrocyclic distortion. A more recent study of Ni MP-11, which has an attached 11 amino acid segment that includes the five-residue CAQCH segment attached to the Ni porphyrin, shows a very nonplanar structure and the alteration of the solution pH changes the degree of the nonplanar distortion under certain conditions (*11*).

SUMMARY AND CONCLUSIONS

NiCyt-*c* exhibits acidic conformational transitions that are similar to those of iron ferricytochrome *c*. At neutral pH, NiCyt-*c* is axially ligated, while at pH extremes, four-coordinate species dominate. The pK_a of histidine/methion-

ine ligand loss is 3.5. At least three conformational states exist in the extremely low pH range from pH 0.5 to 2.8. These forms are all four-coordinate but they differ in the conformation of the porphyrin macrocycle. Upon lowering the pH from 3.0 to 1.0, the amount of the nonplanar conformer decreases relative to that of the planar conformer for NiCyt-*c*. This conformational change is associated with the disruption of the secondary structure and the hydrogen-bond network in the peptide backbone. In agreement with this conclusion, MM calculations on Fe(III) and Ni(II) MP-5 and model porphyrin compounds show that the ruffling dihedral angle of the macrocycle increases as the short, covalently linked peptide segment becomes more established. Normal-coordinate structural decomposition of the structure of Fe(III) MP-5 minimized without the hydrogen bonding shows that the pentapeptide is sufficient to account for the ruffling and most of the minor deformational contributions to the conformation with the exception of saddling. All evidence supports the hypothesis that the small protein segment causes the heme distortion observed in the crystal structures of cytochromes *c*.

ACKNOWLEDGMENT

We thank Professor J. David Hobbs at Montana Tech for helpful discussions in the initial phase of this work.

REFERENCES

1. Geno, M. K., and Halpern, J. (1987) *J. Am. Chem. Soc. 109*, 1238−1240.
2. Barkigia, K. M., Chantranupong, L., Smith, K. M., and Fajer, J. (1988) *J. Am. Chem. Soc. 110*, 7566−7567.
3. Furenlid, L. R., Renner, M. W., Smith, K. M., and Fajer, J. (1990) *J. Am. Chem. Soc. 112*, 1634−1635.
4. Furenlid, L. R., Renner, M. W., Smith, K. M., and Fajer, J. (1990) *J. Am. Chem. Soc. 112*, 8987−8989.
5. Alden, R. G., Ondrias, M. R., and Shelnutt, J. A. (1990) *J. Am. Chem. Soc. 112*, 691−697.
6. Hildebrandt, P., Vanhecke, F., Heibel, G., and Mauk, A. G. (1993) *Biochemistry 32*, 14158−14164.
7. Tetreau, C., Lavalette, D., Momenteau, M., Fischer, J., and Weiss, R. (1994) *J. Am. Chem. Soc. 116*, 11840−11848.
8. Hobbs, J. D., and Shelnutt, J. A. (1995) *J. Protein Chem. 14*, 19−25.
9. Jentzen, W., Ma, J.-G., and Shelnutt, J. A. (1998) *Biophys. J. 74*, 753−763.
10. Anderson, K. K., Hobbs, J. D., Luo, L., Stanley, K. D., Quirke, J. M. E., and Shelnutt, J. A. (1993) *J. Am. Chem. Soc. 115*, 12346−12352.
11. Ma, J.-G., Laberge, M., Jia, S.-L., Vanderkooi, J. M., and Shelnutt, J. A. (1997**)** unpublished experiments.
12. Medforth, C. J., and Smith, K. M. (1990) *Tetrahedron Lett. 31*, 5583−5586.
13. Shelnutt, J. A., Medforth, C. J., Berber, M. D., Barkigia, K. M., and Smith, K. M. (1991) *J. Am. Chem. Soc. 113*, 4077−4087.
14. Shelnutt, J. A., Majumder, S. A., Sparks, L. D., Hobbs, J. D., Medforth, C. J., Senge, M. O., Smith, K. M., Miura, M., Luo L., and Quirke, J. M. E. (1992) *J. Raman Spectrosc. 23*, 523−529.
15. Medforth, C. J., Senge, M. O., Smith, K. M., Sparks, L. D., and Shelnutt, J. A. (1992) *J. Am. Chem. Soc. 114*, 9859−9869.
16. Sparks, L. D., Scheidt, W. R., and Shelnutt, J. A. (1992) *Inorg. Chem. 31*, 2191−2196.
17. Sparks, L. D., Chamberlain, J. R., Hsu, P., Ondrias, M. R., Swanson, B. A., Ortiz de Montellano, P. R., and Shelnutt, J. A. (1993) *Inorg. Chem. 32*, 3153−3163.
18. Sparks, L. D., Medforth, C. J., Park, M.-S., Chamberlain, J. R., Ondrias, M. R., Sengeo, M. O., Smith, K. M., and Shelnutt, J. A. (1993) *J. Am. Chem. Soc. 115*, 581−592.
19. Hobbs, J. D., Majumder, S. A., Luo L., Sickelsmith, G. A., Quirke, J. M. E., Medforth, C. J., Smith, K. M., and Shelnutt, J. A. (1994) *J. Am. Chem. Soc. 116*, 3261−3270.
20. Medforth, C. J., Senge, M. O., Forsyth, T. P., Hobbs, J. D., Shelnutt, J. A., and Smith, K. M. (1994) *Inorg. Chem. 33*, 3865−3872.
21. Jentzen, W., Simpson, M. C., Hobbs, J. D., Song, X., Ema, T., Nelson, N. Y., Medforth, C. J., Smith, K. M., Veyrat, M., Mazzanti, M., Ramasseul, R., Marchon, J.-C., Takeuchi, T., Goddard, W. A., III, and Shelnutt, J. A. (1995) *J. Am. Chem. Soc. 117*, 11085−11097.
22. Song, X.-Z., Jentzen, W., Jia, S.-L., Jaquinod, L., Nurco, D. J., Medforth, C. J., Smith, K. M., and Shelnutt, J. A. (1996) *J. Am. Chem. Soc. 118*, 12975−12988.
23. Findlay, M. C., and Chien, J. C. W. (1977) *Eur. J. Biochem. 76*, 79−83.
24. Babul, J., and Stellwagen, E. (1972) *Biochemistry 11*, 1195−1200.
25. Goto, Y., Calciano, L. J., and Fink, A. L. (1990) *Proc. Natl. Acad. Sci. U.S.A. 87*, 573−577.
26. Goto, Y., Takahashi, N., and Fink, A. L. (1990) *Biochemistry 29*, 3480−3488.
27. Myer, Y. P., and Saturno, A. F. (1991) *J. Protein Chem. 10*, 481−494.
28. Alden, R. G., Crawford, B. A., Doolen, R., Ondrias, M. R., and Shelnutt, J. A. (1989) *J. Am. Chem. Soc. 111*, 2070−2072.
29. Jentzen, W., Unger, E., Karvounis, G., Shelnutt, J. A., Dreybrodt, W., and Schweitzer-Stenner, R. (1996) *J. Phys. Chem. 100*, 14184−14191.
30. Vanderkooi, J. M., Adar, F., and Erecinska, M. (1976) *Eur. J. Biochem. 64*, 381−387.
31. Shelnutt, J. A. (1983) *J. Phys. Chem. 87*, 605−616.
32. Schrötter, H. W., and Klöckner, H. W. (1979) in *Raman Spectroscopy of Gases and Liquids* (Weber, A., Ed.), Chapter 4, pp 123−166, Springer-Verlag, Berlin.
33. Abe, M., Kitagawa, T., and Kyogoku, Y. (1978) *J. Chem. Phys. 69*, 4526−4534.
34. Li, X.-Y., Czernuszewics, R. S., Kincaid, J. R., and Spiro, T. G. (1989) *J. Am. Chem. Soc. 111*, 7012−7023.
35. Li, X.-Y., Czernuszewics, R. S., Kincaid, J. R., Stein, P., and Spiro, T. G. (1990) *J. Phys. Chem. 94*, 47−61.
36. Li, X.-Y., Czernuszewics, R. S., Kincaid, J. R., Su, Y. O., and Spiro, T. G. (1990) *J. Phys. Chem. 94*, 31−47.
37. Mayo, S. L., Olafson, B. D., and Goddard, W. A., III (1990) *J. Phys. Chem. 94*, 8897−8909.
38. Brennan, T. D., Scheidt, W. R., and Shelnutt J. A. (1988) *J. Am. Chem. Soc. 110*, 3919−3924.
39. Rappé, A. K., and Goddard, W. A., III (1991) *J. Phys. Chem. 95*, 3358−3363.
40. Jentzen, W., Song X.-Z., and Shelnutt, J. A. (1997) *J. Phys. Chem. B 101*, 1684−1699.
41. Shelnutt, J. A., Alston, K., Ho, J.-Y., Yu, N.-T., Yamamoto, T., and Rifkind, J. M. (1986) *Biochemistry 25*, 620−627.
42. Choi, S., Spiro, T. G., Langry, K. C., Smith, K. M., Budd, D. L., and La Mar, G. N. (1982) *J. Am. Chem. Soc. 104*, 4345−4351.
43. Song, X., Miura, M., Xu, X., Taylor K. K., Majumder, S. A., Hobbs, J. D., Cesarano, J., and Shelnutt, J. A. (1996) *Langmuir 12*, 2019−2027.
44. Scheidt, W. R., and Lee, Y. (1987) *J. Struct. Bonding 64*, 1−6.
45. Bushnell, G. W., Louie, G. V., and Brayer, G. D. (1990) *J. Mol. Biol. 214*, 585−595.
46. Storm, C. B., Corwin, A. H., Arellano, R. R., Martz, M., and Weintraub, R. (1966) *J. Am. Chem. Soc. 88*, 2525−2532.
47. Shelnutt, J. A., Straub, K. D., Rentzepis, P. M., Gouterman, M., and Davidson, E. R. (1984) *Biochemistry 23*, 3946−3954.
48. Myer, Y. P., and Saturno, A. F. (1990) *J. Protein Chem. 9*, 379−387.
49. Goto, Y., Hagihara, Y., Hamada, D., Hoshino, M., and Nishii, I. (1993) *Biochemistry 32*, 11878−11885.

50. Dickerson, R. E., Tanako, T., Eisenberg, D., Kalli, O. B., Samson, L., Cooper, A., and Margoliash, E. (1971) *J. Biol. Chem. 246*, 1511−1535.
51. Stickle, D. F., Presta, L. G., Dill, K. A., and Rose, G. D. (1992) *J. Mol. Biol. 226*, 1143−1159.
52. Jentzen, W., Unger, E., Song, X.-Z., Jia, S.-L., Schweitzer-Stenner, R., Dreybrodt, W., Scheidt, W. R., and Shelnutt, J. A. (1997) *J. Phys. Chem. A 101*, 5789−5798.
53. Spiro, T. G. (1983) in *Iron Porphyrins, Part Two* (Lever, A. B. P., and Gray, H. B., Ed.) Chapter 3, Addison-Wesley Publishing Company, Reading, MA.
54. Othman, S., Le Lirzin, A., and Desbois, A. (1994) *Biochemistry 33*, 15437−15448.
55. Czernuszewicz, R. S., Li, X.-Y., and Spiro, T. G. (1989) *J. Am. Chem. Soc. 111*, 7024−7031.
56. Shelnutt, J. A., Song, X.-Z., Ma, J.-G., Jia, S.-L., Jentzen, W., and Medforth, C. J. (1998) *Chem. Soc. Rev. 27*, 31−41.

BI972375B